

Atomic force microscopy and surface plasmon resonance investigation of fibronectin interactions with group B streptococci

James R. Hull

National ESCA and Surface Analysis Center for Biomedical Problems and Department of Chemical Engineering, Box 351750, University of Washington, Seattle, Washington 98195-1750

Jared J. Shannon

National ESCA and Surface Analysis Center for Biomedical Problems and Department of Bioengineering, Box 351750, University of Washington, Seattle, Washington 98195-1750

Glen S. Tamura

Division of Infectious Disease and Department of Pediatrics, Children's Hospital and Regional Medical Center and University of Washington, 4800 Sand Point Way NE, Seattle, Washington 98105

David G. Castner^{a)}

National ESCA and Surface Analysis Center for Biomedical Problems, Department of Chemical Engineering, and Department of Bioengineering, Box 351750, University of Washington, Seattle, Washington 98195-1750

(Received 30 March 2007; accepted 19 April 2007; published 11 June 2007)

The interactions of fibronectin (Fn) with group B streptococci (GBS) were investigated using the atomic force microscope (AFM) and surface plasmon resonance (SPR) biosensing. Submonolayer amounts of Fn were immobilized onto the AFM tip by two different methods, using either a sulfosuccinimidyl-4-(*N*-maleimidomethyl) cyclohexane-1-carboxylate (SMCC) linker or a pyridyldithio poly(ethylene glycol) succinimidylpropionate (NHS-PEG-PDP) linker. Each step of both immobilization methods was characterized using x-ray photoelectron spectroscopy. Time-of-flight secondary ion mass spectrometry experiments indicated both methods produced Fn immobilized in a similar conformation. AFM force-distance curves from live GBS plated onto polystyrene exhibited several types of interactions between the Fn functionalized AFM tip and the surface of capsule-deficient GBS (no interactions, interactions with the cell wall, Fn unfolding, large specific unbinding events, and small specific unbinding events). From analysis of the force-distance curves that exhibited only a single specific unbinding event, the work of adhesion and rupture force for the SMCC immobilized Fn tips (11 131 pN nm and 213 pN) were larger than the corresponding values for the NHS-PEG-PDP immobilized Fn tips (8115 pN nm and 189 pN). The unbinding event occurred at distances approximately 100 nm further from the surface with the NHS-PEG-PDP immobilized Fn tip compared to SMCC immobilized Fn tip. The SPR experiments of soluble Fn with adsorbed serine protease C5a peptidase (Scp), the surface protein on GBS that binds Fn, showed that both low (millimolar) and high binding (nanomolar) affinity interactions were present. However, the low binding affinity interactions dominated the adsorption process and, with increasing Fn solution concentration, the amount of Scp bound to Fn via the high binding affinity interaction decreased. These data confirm that Scp binds only to adsorbed Fn at the Fn concentrations typically present in blood plasma. © 2007 American Vacuum Society. [DOI: 10.1116/1.2738854]

I. INTRODUCTION

Bacterial adhesion is mediated by hydrogen bonding,¹ electrostatic interactions,² specific interactions between surface proteins and extracellular matrix proteins,³⁻⁵ and shear forces.⁶ Many bacteria target plasma and extracellular fibronectin (Fn) as an anchoring point for adhesion and invasion of epithelial cells.^{5,7-9} Group B streptococci (GBS) adhere to Fn adsorbed onto a solid substrate, but not soluble Fn.^{10,11} This behavior enables the bacteria to adhere to immobilized Fn in sites where there are large amounts of soluble Fn present, such as the blood stream, or sites of in-

flammation. In addition, this property allows GBS to evade host defenses as Fn acts as an opsonin agent.¹² It is important to quantify the interactions of proteins such as Fn with GBS since GBS is a leading cause of meningitis, pneumonia, and sepsis in neonates and immunocompromised adults in Western countries.^{13,14}

Adherence is thought to be the key step in the initiation of pathogenesis in GBS infections, which following colonization leads to replication and invasion of epithelial cells. The ability to adhere to epithelial cells allows GBS to survive bulk flow defense mechanisms and is thus integral to colonization.¹³ Streptococci and staphylococci frequently express surface adhesins which bind specifically to proteins of the extracellular matrix (ECM), which include fibronectin,

^{a)}Author to whom correspondence should be addressed; electronic mail: castner@nb.engr.washington.edu

laminin, and collagen.¹⁵ Interactions between pathogen adhesin molecules and these ECM proteins are poorly described for all but the fibronectin-adhesin interaction.

Recently, the serine protease C5a peptidase (Scp) was identified as a Fn adhesin for GBS.¹⁶ Scp has a high affinity for adsorbed Fn, and its binding characteristics suggest that there are two possible binding sites for the Scp/Fn interaction.¹⁷ The high affinity binding site has dissociation constant (K_D) of 4 nM, similar to that of other Fn adhesins. In contrast, the low affinity site has K_D in the millimolar range and is unlikely to be of biological significance.

Fibronectin is a large dimeric glycoprotein found in both blood and the extracellular matrix. The monomer units of Fn are joined at the C terminus of the protein in an antiparallel fashion by disulfide bonds.² Each monomer is made up of three modules (Fn types I, II, and III) and a variable region. Fn I and II have interchain disulfide bonds, while type III does not. The variable unit of Fn does not contain any of the three modules. In its soluble form, Fn is globular with a radius of roughly 20 nm, while in the adsorbed state, it can take on a number of different conformations ranging from globular to elongated and cross-linked,^{18–20} based on the surface properties of the substrate.

The atomic force microscope (AFM) and the surface plasmon resonance (SPR) biosensor are ideal tools to study bacterial/protein interactions. The high spatial resolution and force sensitivity of the AFM (Refs. 21–23) allow for imaging with nanometer scale resolution and measuring interactions between biological molecules in the piconewton range. SPR can measure, in real time, dynamic interactions between ligands immobilized on a surface and its receptor in solution.^{3,4}

Several different approaches are used to study bacterial interactions with the AFM: probing a live microbe with a receptor attached to the AFM tip,^{24,25} bacterial interactions with surfaces by either fixing the bacteria to the probe²⁶ or using a specific tip to probe immobilized bacteria,²⁷ using the AFM to scrape the bacteria off the surface²⁸ to measure adhesion forces, using the AFM to measure the elasticity of the bacterial cell membrane,^{29,30} and probing the surface charge.³¹

In this work, we investigate the specificity of Fn with live GBS. GBS were imaged and probed with Fn bound to an AFM via two immobilization strategies. X-ray photoelectron spectroscopy (XPS) and time-of-flight secondary ion mass spectrometry (ToF-SIMS) were used to verify the surface modifications to the AFM tip. Surface plasmon resonance was used to probe the interactions of soluble Fn with immobilized Scp.

II. EXPERIMENT

A. Bacterial strains and plasmids

GBS was grown, and the phage display fragment of Scp that is responsible for Fn binding (Scp-pdf) was purified as glutathione S-transferase fusion protein as described by Tamura *et al.*¹⁷ One caveat when probing the bacteria with a

specific receptor is that the strain of bacteria must be capsule deficient to avoid tip interactions with the capsule. Capsule-deficient GBS were used in this study.

B. Surface plasmon resonance

Surface plasmon resonance was performed using a prototype of the Plasmon-II system.³² The light source for this SPR uses *p*-polarized white light passed through a planar prism (Kretschmann) configuration and projected onto the back of a gold-coated glass slide at a fixed angle (96.5°). Reflected light was collected in a spectrophotometer connected to a personal computer with monitoring software. A dual channel flow cell was used, with one channel as the reference to track drift and the other channel for sensing. A peristaltic pump was used to deliver the protein solution through the flow cell at a rate of 50 μ l/min. Glass SPR chips were cleaned prior to gold deposition. Chips were sonicated twice in RBS 35 detergent (Pierce, Rockford, IL) for 5 min, rinsed twice in 18 M Ω water, sonicated twice in 18 M Ω water for 5 min, sonicated twice in acetone for 5 min, sonicated twice in methanol for 5 min, and then dried with nitrogen. Gold was deposited onto the chips by electron beam evaporation at pressures below 10⁻⁶ Torr. A 2 nm layer of chromium was deposited first as an adhesion layer, and then a 48 nm layer of gold was subsequently deposited. Chips were UV ozone cleaned prior to use. Recycled chips were cleaned with a solution consisting of 7:3 (v:v) sulphuric acid and 30% hydrogen peroxide solution and then UV ozone treated prior to use. Human plasma fibronectin (Invitrogen, Carlsbad, CA), casein (Pierce, Rockford, IL), rat tail type I collagen (BD Biosciences, Bedford, MA), and the Scp-pdf fusion were all stored in degassed 1X phosphate buffered saline of (PBS) of pH 7.4 at 4 °C during experiments. Fn was passed through a 0.2 μ m filter to remove protein aggregates before use.

C. X-ray photoelectron spectroscopy

The XPS measurements were performed on a Surface Science Instrument S-Probe spectrometer (Mountain View, CA) equipped with monochromatic Al $K\alpha$ source (kinetic energy = 1486.6 eV), hemispherical analyzer, and multichannel detector. The binding energy (BE) scale was referenced by setting the C_{1s} BE to 285.0 eV. Elemental compositions were determined from spectra acquired at an analyzer pass energy of 150 eV. High-resolution spectra were obtained using an analyzer pass energy of 50 eV. Further details of the XPS experiments are published elsewhere.³³

D. Time-of-flight secondary ion mass spectrometry

A model 7200 Physical Electronics instrument (PHI, Eden Prairie, MN) was used for ToF-SIMS data acquisition. The instrument has an 8 KeV Cs⁺ ion source, a reflectron time-of-flight mass analyzer, chevron-type multichannel plates, and a time-to-digital converter. Data were acquired over a mass range from $m/z=0$ to 1500 for both positive and negative secondary ions. The area of analysis for each spectrum

was $100 \times 100 \mu\text{m}^2$. The total ion dose used to acquire each spectrum was less than 2×10^{12} ions/cm². The ion beam was moved to a new spot on the sample for each spectrum with a total of three spots per sample. The mass resolution ($m/\Delta m$) of the secondary ion peaks was typically between 5000 and 6000. At least three samples were prepared for each step in the modification process. The mass scale for the positive spectra was calibrated using CH_3^+ , C_2H_3^+ , and C_3H_5^+ peaks, and the mass scale for the negative spectra was calibrated using CH^- , OH^- , and C_2H^- . The differences between the expected and observed masses for both positive and negative ions after calibration were less than 10 ppm.

E. Atomic force microscopy

GBS strain COH1 were grown in trypticase soy broth at 37 °C to an absorbance of 0.6 A at 600 nm. 1 ml was then centrifuged for 30 s at 13.2 krpm, and the supernatant discarded. The pellet was then resuspended in 1 ml PBS and centrifuged for an additional 30 s at 13.2 krpm, and the supernatant discarded. The pellet was again resuspended in 1 ml PBS, then 100 μl of this solution was diluted in 900 μl PBS. Approximately 500 μl was then pipetted onto polystyrene and allowed to adsorb for 1 h on ice. After 1 h the solution was rinsed off with PBS, and the polystyrene was submerged in PBS until AFM analysis. AFM analysis was performed immediately following adsorption, and force curve collection was completed within 3 h.

The AFM used in this study was a Molecular Imaging PicoScan (Pheonix, AZ). GBS imaging was performed in contact mode. Force experiments were carried out with NP-S tips (Veeco, Santa Barbara, CA), with spring constants in the range 0.06–0.52 N/m. Spring constants were measured by the thermal noise method.³⁴ Force curves were carried out at a rate of 1 Hz with a force trigger of 0.25 V and a total travel distance of 1 μm . For each experiment there were between 500 and 625 force curves obtained. The tip location was controlled with a script to raster the tip over the sample area. All force curves were taken under PBS.

Jump heights were extracted from the force curves by filtering them to exaggerate vertical segments with a filter proposed by Kasas *et al.* (–2, –5, –8, –10, 0, 5, and 20).³⁵ Once the peaks were found, 11 points to the left and right of the peak were fitted with a second-degree polynomial, and the difference between the end points of the polynomials was taken as the jump height. This method was proposed by Baumgartner *et al.*³⁶ The point of contact was estimated as the intersection of lines constructed from the undeflected cantilever and the steepest part of the compliance region.³⁶ This analysis routine was written in JAVA as a plugin for IMAGEJ.

F. SMCC surface functionalization

AFM tips were rinsed with ethanol, then cleaned in piranha solution (7:3 H_2SO_4 : 30% hydrogen peroxide) for 3 h prior to protein adsorption. Samples were then rinsed with water and dried/stored in nitrogen gas

until adsorption. Si_3N_4 AFM tips were incubated in 0.1% (v/v) (aminoethylaminomethyl)-phenethyltrimethoxysilane (AEAMPE, Gelest, Tullytown, PA) in chloroform (J.T. Baker, Phillipsburg, NJ) for 1 h. Tips were rinsed with water, then incubated in 1 mg/ml sulfosuccinimidyl-4-(*N*-maleimidomethyl) cyclohexane-1-carboxylate (SMCC, Pierce, Rockford, IL) in water for 1 h. Then tips were rinsed with water and incubated in 0.1 mg/ml Fn in water for 1 h. Finally, tips were rinsed with copious amounts of water and kept submerged until use. The same functionalization was performed on Si_3N_4 chips, with XPS performed on two samples after each step.

G. NHS-PEG-PDP surface functionalization

Esterification of the AFM tips was carried out by condensing ethanolamine HCl (Sigma, Milwaukee, WI) with the silanol groups on silicon nitride. This procedure was first proposed by Hinterdorfer *et al.*³⁷ First, all of the glassware used for esterification were baked dry along with the molecular sieves (Fisher Scientific). Then, the ethanolamine HCl was dissolved in dimethyl sulfoxide (DMSO) (J.T. Baker, Phillipsburg, NJ) at a 30% (wt/wt) solution with the molecular sieves. Once the ethanolamine HCl was dissolved and the molecular sieves stopped offgassing, the tips and blanks were introduced. The reaction was allowed to proceed overnight. Following esterification, the tips and blanks were rinsed in fresh DMSO followed by chloroform.

Next, the substrates were incubated for 4 h in a solution of 1 mg/ml of pyridyldithio poly(ethylene glycol) succinimidylpropionate³⁸ (NHS-PEG-PDP, Polypure, Oslo, Norway) in chloroform with 1% (v/v) triethylamine (Sigma, Milwaukee, WI) as catalyst. This step binds the NHS of the PEG chain to the primary amines on the surface. Substrates were then incubated in 0.1% (v/v) 2-[methoxy(polyethylenoxy)propyl]-trimethoxysilane (Gelest, Tullytown, PA) in chloroform for 1 h to cover any unfunctionalized regions of the substrates with PEG. Substrates were then rinsed with water and incubated in 0.1 mg/ml Fn in PBS for 1 h. The AFM tips were then rinsed with copious amounts of water and kept submerged in water until use.

As a control, following Fn functionalization a few of the tips were incubated in 0.1 mg/ml Scp-pdf for 1 h. The tips were again rinsed with copious amounts of water and stored under water prior to use.

H. Live bacteria assay

An assay was performed to verify that live cells were present during AFM analysis. This was accomplished by performing seven adsorptions on polystyrene substrates as described above. Every half hour following adsorption (from 0 to 3 hours), 400 μl trypsin/ethylenediamine tetra-acetic acid solution was applied to one plate at 37 °C for 3 min. The plate was tapped to help loosen cells. The trypsin solution was then pipetted off, and 100 μl of this solution was diluted in 900 μl PBS. From this solution, 100 μl was plated

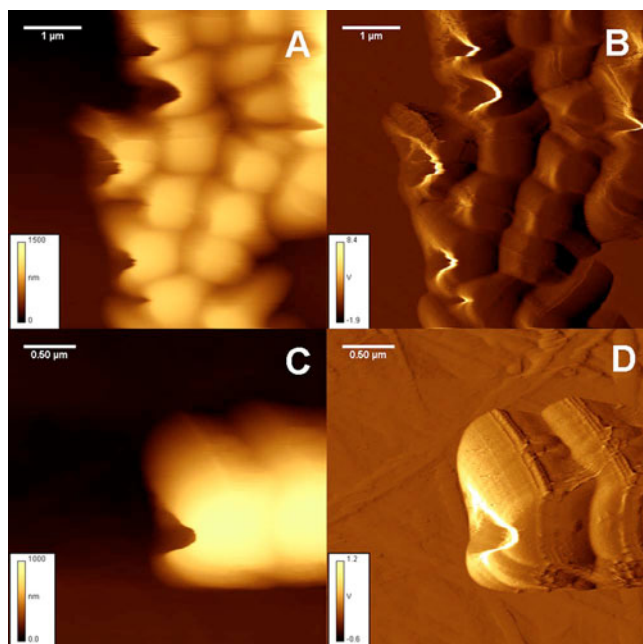


FIG. 1. Live group B streptococci imaged with contact mode AFM. (A) Topographic images ($z=0-1500$ nm) and (B) deflection images ($z=-1.9-8.4$ V) of a group of GBS. (C) Topographic images ($z=0-1000$ nm) and (D) deflection images ($z=-0.6-1.2$ V) of two GSB. The deflection images show sloping sides due to the shape of the AFM tip.

on Todd-Hewitt agar and incubated overnight at 37 °C. The resultant colonies from each of the seven plates were counted.

III. RESULTS AND DISCUSSION

A. Live bacteria assay

First, live adherent bacteria were quantified at various time points to show the bacteria had not died over the course of the AFM experiments. At all time points, there were at least 150 CFU (colony-forming unit) on all samples with no time dependence trend. This indicates that the bacterial were alive during the time course of the experiments.

B. AFM imaging

Contact mode AFM was then used to image the bacteria, with the force set point set to a minimum force to maintain contact. Figure 1 shows typical AFM images of the live bacteria. The shape of the bacteria is spherical with a circumferential cleft. The bacteria are roughly 1 μm in height with a length of 500 nm. The deflection images show a sloping side. This is due to the pyramidal shape of the tip, which is 2.5–3.5 μm high. The side of the tip contacts the bacteria before the apex of the tip, which results in the sloping sides observed in the deflection image. The cleft on the bug is clearly visible in the deflection image, but it is washed out in the topographical image. The topographical image provides a clearer representation of the outline and footprint of the bacteria, but the deflection image shows much greater surface detail. Typically, GBS assembles into chains;³⁹ however, in

this study only individual or clusters of GBS were observed. This is likely due to the deposition method used in this study. These results demonstrate that we were able to make high-resolution topographic images of live GBS on polystyrene.

C. Fibronectin immobilization

We wanted to define the reason why GBS binds only to immobilized Fn. Was it conformational changes that occur only after adsorption of Fn to a solid substrate or the mobility of Fn? To test these possibilities, we first sought to define two methods for immobilizing Fn onto the AFM tip. The first chemistry uses AEAMPE, then SMCC, to link the Fn to the tip, which would result in multiple anchoring points for Fn, resulting in Fn being immobile on the surface. Figure 2 shows the SMCC immobilization strategy along with the corresponding XPS high-resolution carbon spectra. After the amino silane functionalization, an increase in the hydrocarbon and amine carbon is observed in the C1s spectrum. Likewise, there is an increase in the carboxylate carbon with the addition of the SMCC and an increase in the amide carbon with the addition of Fn. The atomic percentage of nitrogen measured by XPS after Fn immobilization was 4.0 at. %, indicating that the tip is not fully covered by Fn. The atomic percentage of nitrogen in Fn is approximately 15%. Since a monolayer of Fn is typically thinner than the sampling depth of XPS, the measured atomic percentage of nitrogen will be lower than 15%.

The second chemistry uses a heterobifunctional cross-linker, NHS-PEG-PDP, to link Fn to the AFM tip. This chemistry results in sparse coverage of this flexible linker, which allows Fn some movement. First, primary amines were introduced to the surface by the ethanolamine HCl treatment, then the NHS-PEG-PDP was bound to the surface primary amines through the NHS group. A shorter chain PEG silane was used to backfill any regions of the tip not covered with NHS-PEG-PDP to help reduce nonspecific adhesion. Fn was introduced in the last step. Figure 3 shows the XPS high-resolution carbon spectra after each step in this modification. There is an increase in the ether carbon contribution with the addition of PEG and an increase in the amide carbon with the addition of Fn. The amount of nitrogen detected by XPS from Fn attached via NHS-PEG-PDP is slightly higher (5.0 at. %) than Fn attached via SMCC. For both immobilization methods, the amount of Fn attached to the tip is less than a monolayer.

ToF-SIMS was used to determine whether or not similar conformation and orientation of Fn were obtained from the two different immobilization methods. It has been shown that the relative ToF-SIMS intensities from the amino acid fragments in the protein depend on protein conformation and orientation.⁴⁰ For example, as proteins denature the intensities of fragments from hydrophobic amino acids tend to increase relative to the intensities of the hydrophilic amino acids.^{41–43} Previously we have shown that the peak intensities of the sulfur containing amino acid fragments (Met and Cys) and selected hydrophobic amino acids (Gly, Leu, and Ile) exhibit the largest changes as the conformation of Fn

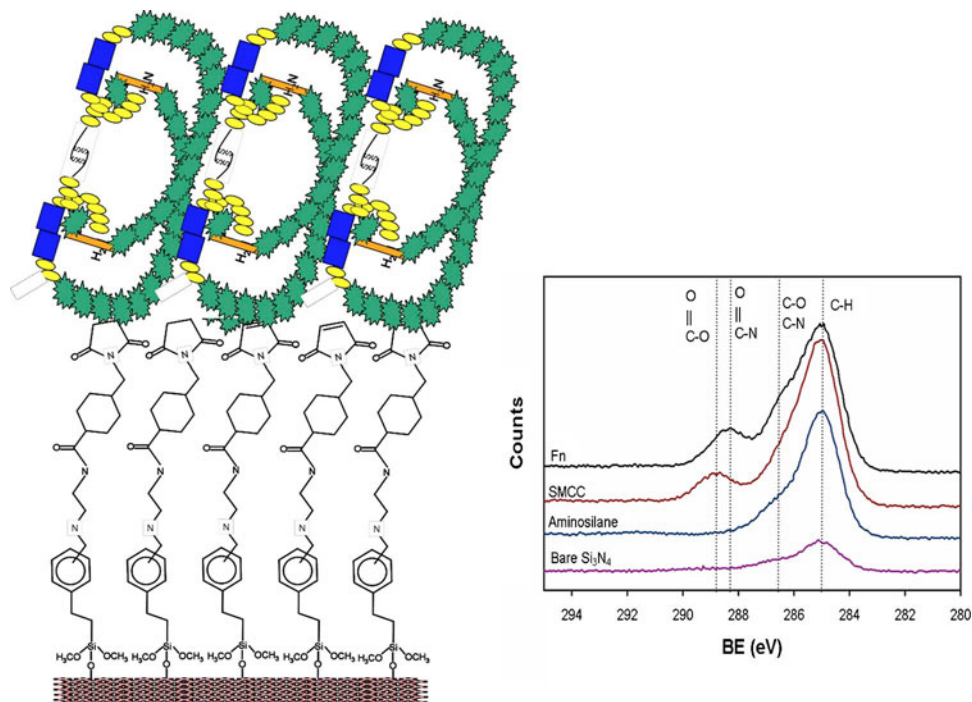


FIG. 2. Schematic showing Fn conjugation via SMCC. The high-resolution carbon spectra show the introduction of key functional groups for each step. There is an increase in the CN peak with the introduction of the amino silane. The carboxyl peak increases with the introduction of the SMCC and the amide peak increases with the introduction of Fn.

changes.⁴⁴ Thus, the ToF-SIMS intensities of fragments from these amino acids are shown in Fig. 4. From the ToF-SIMS results shown in Fig. 4, it is apparent that there are no significant differences in conformation for Fn immobilized by the two different surface modifications. There are two possible explanations for this observation. First, both immobili-

zation strategies rely on linking Fn via formation of a disulfide bond, so the attachment of Fn should be similar for both methods. Second, extensive denaturation of Fn by drying and insertion to the ultrahigh vacuum ToF-SIMS chamber could make it difficult to observe any conformation differences that

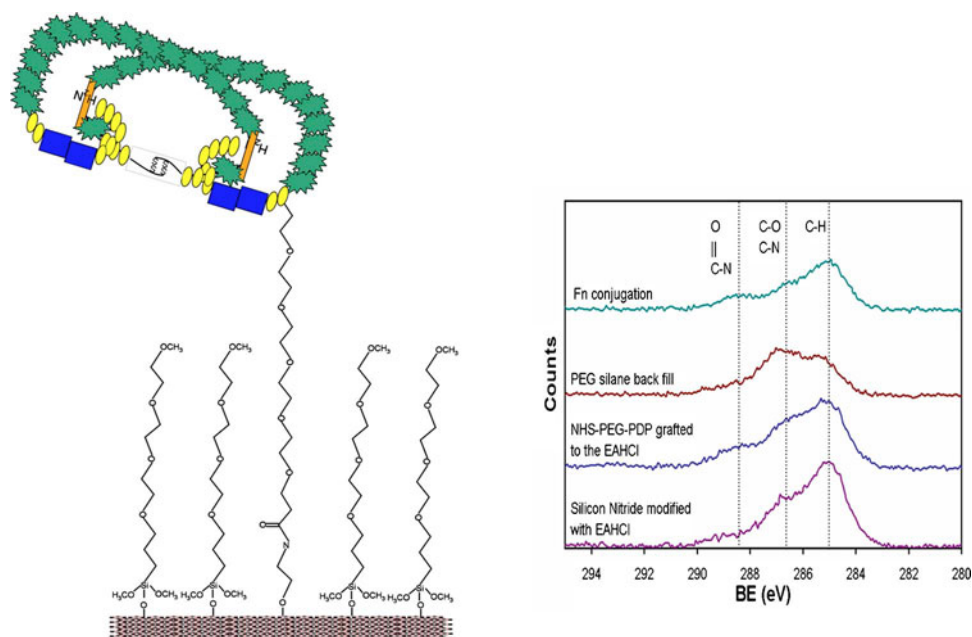


FIG. 3. Schematic showing Fn conjugation via PEG. The high-resolution carbon spectra show the introduction of key functional groups for each step. There is a slight increase in the amine bond with the introduction of the ethanolamine. The ether carbon peak increases with the introduction of the PEG and the amide bond appears with the introduction of Fn.

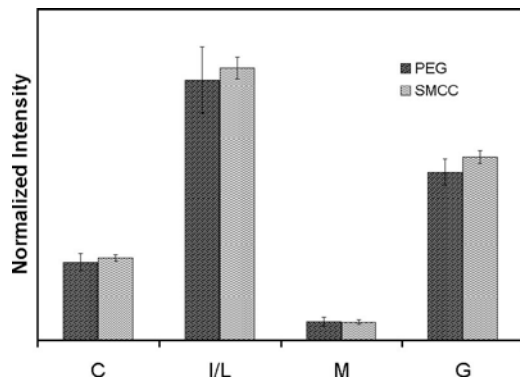


FIG. 4. Relative ToF-SIMS peak intensities of the Met, Cys, Leu/Ile, and Gly amino acids from Fn immobilized via NHS-PEG-PDP (left) and SMCC (right) linkers.

might exist prior to drying Fn. However, it has been shown that a dense PEG surface inhibits denaturation of proteins during drying for ToF-SIMS analysis.⁴³

These results indicated that the immobilization via these two methods resulted in similar conformation and orientations, thus allowing us to use these two methods to test the effect of immobilization method apart from secondary structural changes on the ability of GBS to bind to Fn.

D. Force spectroscopy

After imaging the bacteria, force curves were performed in a raster fashion over a region of interest that included the bacteria. Figure 5 shows the five types of force curves observed in this data set: (A) no interactions, (B) interactions with the cell wall, (C) unfolding of the Fn upon retraction of the tip, (D) large unbinding events, and (E) small unbinding events. Besides the five characteristic curves, there were curves that exhibit combinations, such as cell wall interactions and Fn unfolding. Interactions with the cell wall manifest itself as discontinuities in the compliance region of the curve. As the probe is pushed into the cell wall, it breaks

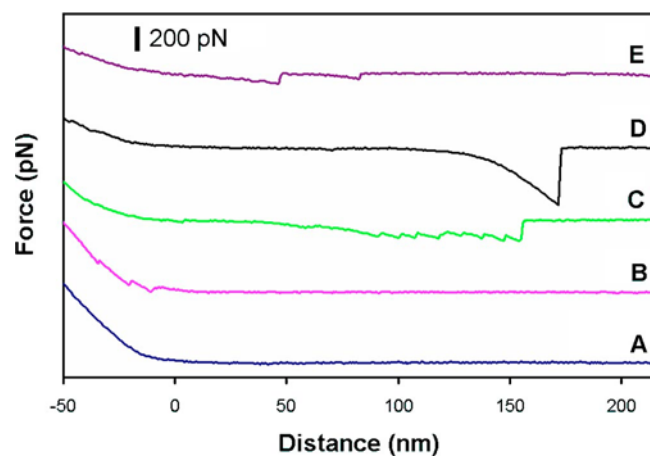


FIG. 5. Representative force-distance curves for SMCC immobilized Fn AFM tips interacting with GBS. (A) No interactions, (B) interactions with the cell membrane, (C) Fn unfolding, (D) large adhesive events, and (E) small adhesive events.

through it, resulting in the observation of interactions in both the approach and retraction cycles. AFM studies of lipid bilayers have observed the same phenomena: when the tip breaks through the layers of the lipid bilayer, there are two distinct discontinuities in the compliance region.⁴⁵ Fibronectin unfolding exhibits itself as a sawtooth pattern in the retraction portion of the force curve.^{46–48} Even though Fn was observed unfolding during the experiment, this does not effect the binding of subsequent force-distance curves because Fn spontaneously refolds during the course of spectroscopy experiments.⁴⁶ The fact that there was no observed dependence of the interactions on the repetition number for the force spectroscopy experiments in our study is consistent with Fn refolding between force curves. Before the force curve analysis, curves that were not located on the bacteria were discarded. The slope of the force curve in the compliance region was used as the criteria for determining whether or not a force curve was located on the bacteria. Force curves taken on the substrate exhibit a significantly steeper slope in the compliance region since the substrate is harder than the bacteria. The variance in the compliance region of the force curves on GBS is due to the cell surface being inhomogeneous and the mechanical response of the cell wall when probed. To ensure that these interactions are specific for Fn, the Fn functionalized tip was blocked with Scp-pdf (the Fn receptor on the bacteria).¹⁶ After Scp-pdf blocking, there were no interactions observed in the force curves. The strain of GBS used was capsule deficient, so the interactions measured by Fn functionalized tip were with the cell surface and associated surface proteins.

For analysis of the force curves, specific interactions were assumed to take place only between a Fn molecule on the AFM tip and a Scp-pdf molecule on the surface of the bacteria. Thus, force curves that exhibit one interaction beyond the point of contact were assumed to be specific interactions. Both the large and small unbinding events that were observed can be attributed to the specific interactions between Fn and Scp-pdf. However, even though the specific unbinding events were observed in combination with protein unfolding and nonspecific interactions near the point of contact, only the last unbinding events were used to calculate the interaction forces.

The percentage of force curves on the bacteria that corresponded to single unbinding events were 13% (SMCC immobilization) and 17% (NHS-PEG-PDP immobilization). Examples of the force curves used to calculate the work of adhesion and rupture force are shown in Figs. 6 and 7. The length scale over which the interactions occur is larger than the individual proteins and linkers themselves. This is due to unfolding of the proteins involved in the interaction and the flexibility of the cell wall.

For force curves exhibiting a single unbinding event, this unbinding event was found to occur at a similar distance from the point of contact for the set of force curves acquired with each type of Fn functionalized tip. However, the location of this unbinding event differed for AFM tips with Fn immobilized by the NHS-PEG-PDP method compared to the

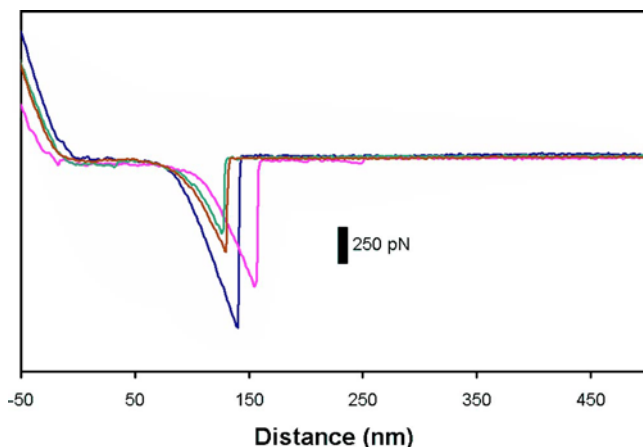


FIG. 6. Force-distance curves that exhibit specific interactions between Fn on the AFM tip and Scp on the surface of GBS. The Fn was immobilized onto the tip with a SMCC linker.

SMCC method (see Figs. 6 and 7). The observation of the unbinding occurring at larger distances for Fn tips functionalized with the NHS-PEG-PDP method is consistent with the fact that the PEG linker is longer than the SMCC linker.

The work of adhesion and the rupture force for the SMCC and PEG functionalized tips are summarized in Table I. The rupture force and work of adhesion were greater with SMCC than those found for PEG functionalized tips. ToF-SIMS indicated that the Fn conformation and orientation were similar for the two types of immobilization methods. However, it is apparent from the force curves that the presence of the PEG chains also plays a role in determining the Fn interactions with the surface of the bacteria. As PEG is well known to inhibit protein adsorption,^{49,50} it is not surprising that the measured work of adhesion and rupture forces were lower for Fn immobilized to a PEG surface.

The distribution of forces observed for both immobilization strategies indicate that differences in rupture force and work of adhesion are statistically different for the two immobilization strategies that allow different amounts of Fn mo-

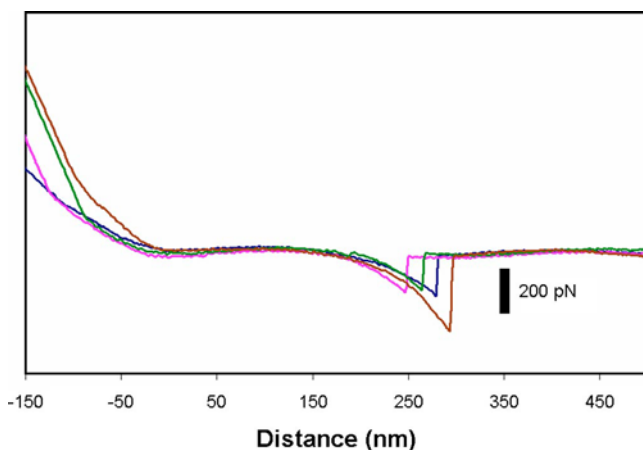


FIG. 7. Force-distance curves that exhibit specific interactions between Fn on the AFM tip and Scp on the surface of GBS. The Fn was immobilized onto the tip with a NHS-PEG-PDP linker.

TABLE I. Summary of Fn rupture data determined from force spectroscopy experiments. The standard deviations are shown in parentheses.

	Rupture force (pN)	WOA (pN nm)	Frequency (%)
SMCC	213 (98)	11 131 (4300)	13
PEG	189 (49)	8115 (4500)	17

bility due to the different chain lengths of the cross-linkers. However, ToF-SIMS indicates that the secondary structure of Fn on the AFM tip is the same for both immobilization strategies. Taken together, these results suggest that the binding of GBS to Fn is mediated by how the Fn is bound to a surface and its mobility, when the conformation and orientation of the Fn are similar.

E. Surface plasmon resonance

By immobilizing Fn to an AFM tip, regardless of the chemistry used, there will be some changes in the structure and conformation of the Fn molecule from its native state in solution. Thus, SPR was used to investigate the interaction of Scp-pdf expressed at the surface of GBS with truly soluble Fn. For this study the Scp-pdf fusion protein was first adsorbed onto the sensor surface, then blocked with casein prior to flowing a solution of Fn over the sensor. Figure 8 shows a typical SPR sensogram for this sequence of experiments. Adsorbed collagen (Col), which binds soluble Fn, was used as a positive control. Fn uptake onto both the Scp-pdf and collagen surface exhibited two regimes, an initial rapid increase in Fn accumulation followed by a region of little or no Fn accumulation. The magnitude of Fn accumulation in the initial regime increased linearly with Fn solution concentration, which can be attributed to two different effects: the refractive index change due to switching from pure buffer to the Fn solution and Fn binding to the surface. The second part of the curve is likely due to rearrangement of the surface proteins and results in slower Fn adsorption. Most of the Fn is removed from the Scp-pdf upon rinsing, indicating a very weak binding interaction between soluble Fn and Scp-pdf. The small amount of Fn remaining on the Scp-pdf surface after rinsing decreased with increasing Fn solution concentration. In contrast, significantly more Fn remained on the Col surface after rinsing and exhibited a maximum at an intermediate Fn solution concentration. Both Col/Fn (Ref. 51) and Scp/Fn (Ref. 17) have low and high affinity binding sites, and it is thought that the fast initial uptake of Fn is dominated by the low affinity binding interaction. In the slow uptake region, structural rearrangement of Fn to expose the high affinity site occurs. The more low affinity Fn bound to the Scp-pdf surface, the more difficult it is for Fn to restructure and expose its high affinity binding site. This is consistent with the observed decrease in the amount of high affinity Fn binding as the amount of low affinity Fn binding increases. At the concentration of Fn in plasma ($\sim 300 \mu\text{g/ml}$),⁵² the high affinity binding sites will be blocked and GBS will not be able to tightly bind soluble Fn, as observed.

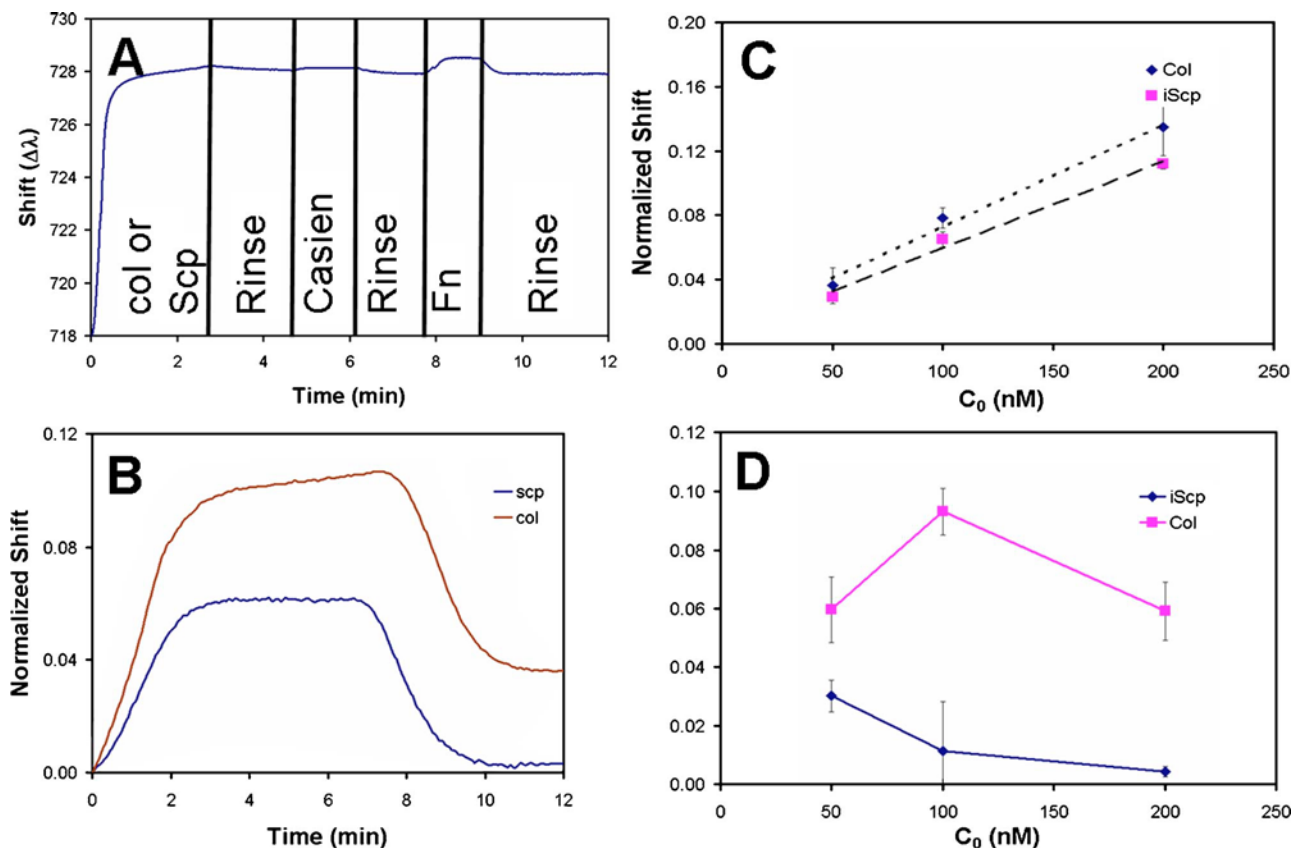


FIG. 8. Interaction of soluble Fn with adsorbed Scp and Col. (A) A SPR sensogram showing all steps in the process. (B) Typical uptake curves observed for Fn interacting with adsorbed Scp and Col. (C) A plot showing the linear increase in the amount of Fn adsorbed in the initial uptake region. (D) The amount of Fn remaining bound to Scp and Col after rinsing.

IV. CONCLUSIONS

Contact mode AFM imaging is a reliable and reproducible method of imaging live GBS adsorbed onto polystyrene. Topographic images provided more realistic footprints of GBS, while deflection images provided higher resolution images of surface features. AFM force curves acquired using Fn functionalized tips to probe capsule-deficient GBS (as determined from the slope in the compliance region of the force curve) exhibited no interactions, interactions with the cell wall, Fn unfolding, large specific unbinding events, and small specific unbinding events. Although ToF-SIMS indicated that the conformation of Fn was similar whether immobilized with a SMCC or NHS-PEG-PDP linker, the measured work of adhesion and rupture forces were smaller for the NHS-PEG-PDP immobilized Fn tips. The longer NHS-PEG-PDP linker also resulted in the specific unbinding events occurring at distances further from the surface. These results suggest that the mobility of Fn on a surface results in a slightly lower interaction with Scp-pdf as opposed to Fn bound to the surface with a shorter cross-linker. Control experiments using Scp-pdf attached to the Fn on the AFM tips showed that the binding of Fn with GBS is specific and likely occurs through interactions with Scp-pdf. SPR showed that low binding affinity interactions dominated the Fn adsorption of soluble Fn

onto a Scp-pdf covered surface. As the Fn solution concentration was increased, the Fn restructuring required to expose the high binding affinity site was blocked.

ACKNOWLEDGMENTS

Support for this research was provided by the National ESCA and Surface Analysis Center for Biomedical Problems (funded by NIH Grant No. EB-002027) and the University of Washington, Engineered Biomaterials program (funded by NSF Grant No. EEC-95291661). One of the authors (J.R.H.) was supported by a NIH predoctoral traineeship from Grant No. GM-065098. Another author (J.J.S.) was supported by a NIH undergraduate traineeship from Grant No. DK-070082. The authors would also like to thank Donald Chaffen and David Carol at the Seattle Biomedical Research Institute for assistance in growing GBS.

- ¹Nehal I. Abu-Lail and Terri A. Camesano, *Langmuir* **22**, 7296 (2006).
- ²Seong Soo A. An, Jesus Jimenez-Barbero, Torben E. Peterson, and Miguel Llinas, *Biochemistry* **31**, 9927 (1992).
- ³Hyeon J. Joh, Karen House-Pompeo, Joseph M. Patti, S. Gurusiddappa, and Magnus Hook, *Biochemistry* **33**, 6086 (1993).
- ⁴Bernd Kreikemeyer, Sonja Oehmcke, Masanobu Nakata, and Raimund Hoffrogge, *J. Biol. Chem.* **279**, 15850 (2004).
- ⁵Joseph M. Patti, Bradley L. Allen, Martin J. McGavin, and Magnus Hook, *Annu. Rev. Microbiol.* **48**, 585 (1994).

- ⁶Wendy E. Thomas, Elna Trintchina, Manu Forero, Viola Vogel, and Evgeny V. Sokurenko, *Cell* **109**, 913 (2002).
- ⁷B. Brett Finlay and Stanley Falkow, *Microbiol. Rev.* **53**, 210 (1989).
- ⁸K. S. Doran and V. Nizet, *Mol. Microbiol.* **54**, 23 (2004).
- ⁹Danny Joh, Elisabeth R. Wann, Bernd Kreikemeyer, Pietro Speziale, and Magnus Hook, *Matrix Biol.* **18**, 211 (1999).
- ¹⁰Karina M. Butler, Carol J. Baker, and Morven S. Edwards, *Infect. Immun.* **55**, 2404 (1987).
- ¹¹G. S. Tamura and C. E. Rubens, *Mol. Microbiol.* **15**, 581 (1995).
- ¹²J. Morehead, I. Coppens, and N. W. Andrews, *Infect. Immun.* **70**, 4571 (2002).
- ¹³Glen S. Tamura, Aphakorn Nittayajarn, and Deborah L. Schoentag, *Infect. Immun.* **70**, 2877 (2002).
- ¹⁴Monica M. Farley, Christopher Harvey, Tina Stull, J. David Smith, Anne Schuchat, Jay D. Wenger, and David S. Stephens, *N. Engl. J. Med.* **328**, 1807 (1993).
- ¹⁵B. Westerlund and T. K. Korhonen, *Mol. Microbiol.* **9**, 687 (1993).
- ¹⁶C. Beckmann, J. D. Waggoner, T. O. Harris, G. S. Tamura, and C. E. Rubens, *Infect. Immun.* **70**, 2869 (2002).
- ¹⁷G. S. Tamura, J. R. Hull, M. D. Oberg, and D. G. Castner, *Infect. Immun.* **74**, 5739 (2006).
- ¹⁸Jurgen Engel, Erich Odermatt, and Andreas Engel, *J. Mol. Biol.* **150**, 97 (1981).
- ¹⁹R. Emch F. Zenhausern, M. Jobin, M. Taborelli, and P. Descouts, *Ultramicroscopy* **42–44**, 1155 (1992).
- ²⁰Kamin J. Johnson Harvey Sage, Gina Briscoe, and Harold P. Erickson, *J. Biol. Chem.* **274**, 15473 (1999).
- ²¹Jan H. Hoh, Jason P. Cleveland, Craig B. Prater, Jean-Paul Revel, and Paul K. Hansma, *J. Am. Chem. Soc.* **114**, 4917 (1992).
- ²²G. Binnig, C. Gerber, E. Stoll, T. R. Albrecht, and C. F. Quate, *Surf. Sci.* **189–190**, 1 (1987).
- ²³G. K. Binnig, *Phys. Scr.*, T **T19A**, 53 (1987).
- ²⁴Vincent Dupres, Franco D. Menozzi, Camille Loch, Brian H. Clare, Nicholas L. Abbott, Stephane Cuenot, Coralie Bompard, Dominique Raze, and Yves F. Dufrene, *Nat. Methods* **2**, 515 (2005).
- ²⁵Yasser Bustanji, Carla Renata Arcciola, Matteo Conti, Enrico Mandello, Lucio Montanaro, Bruno Samori, *Proc. Natl. Acad. Sci. U.S.A.* **100**, 13292 (2003).
- ²⁶Haiying Tang Ting Cao, Xuemei Liang, Anfeng Wang, Gregory W. Auner, Steven O. Salley, and K. Y. Simon Ng, *Biotechnol. Bioeng.* **94**, 167 (2006).
- ²⁷Xu Li and Bruce E. Logan, *Langmuir* **20**, 8817 (2004).
- ²⁸Kathryn A. Whitehead, Dale Rogers, John Colligon, Chris Wright, and Joanna Verran, *Colloids Surf., B* **51**, 44 (2006).
- ²⁹M. A. Beckmann, S. Venkataraman, M. J. Doktycz, J. P. Nataro, C. J. Sullivan, J. L. Morrell-Falvey, and D. P. Allison, *Ultramicroscopy* **106**, 695 (2006).
- ³⁰Ahmed Touhami, Bernard Nysten, and Yves F. Dufrene, *Langmuir* **19**, 4539 (2003).
- ³¹Francois Ahimou, Frederic A. Denis, Ahmed Touhami, and Yves F. Dufrene, *Langmuir* **18**, 9937 (2002).
- ³²Jiri Homola, Jakub Dostalek, Shengfu Chen, Avraham Rasooly, Shaoyi Jiang, and Sinclair S. Yee, *Int. J. Food Microbiol.* **75**, 61 (2002).
- ³³Buddy D. Ratner, Deborah Leach-Scampavia, and David G. Castner, *Biomaterials* **14**, 148 (1993).
- ³⁴Jeffrey L. Hutter and John Bechhoefer, *Rev. Sci. Instrum.* **64**, 1868 (1993).
- ³⁵Sandor Kasas, Beat M. Riederer, Stefan Catsicas, Brunero Cappella, and Giovanni Dietler, *Rev. Sci. Instrum.* **71**, 2082 (2000).
- ³⁶W. Baumgartner, P. Hinterdorfer, and H. Schindler, *Ultramicroscopy* **85**, 85 (2000).
- ³⁷P. Hinterdorfer, K. Schilcher, W. Baumgartner, H. J. Gruber, and H. Schindler, *Nanobiology* **4**, 177 (1998).
- ³⁸T. Haselgrubler, A. Amerstorfer, and H. J. Gruber, *Bioconjugate Chem.* **6**, 242 (1995).
- ³⁹F. J. Picard and M. G. Bergeron, *Eur. J. Clin. Microbiol. Infect. Dis.* **23**, 665 (2004).
- ⁴⁰C. D. Tidwell, D. G. Castner, S. L. Golledge, B. D. Ratner, K. Meyer, B. Hagenhoff, and A. Benninghoven, *Surf. Interface Anal.* **31**, 724 (2001).
- ⁴¹Nan Xia, Collin J. May, Sally L. McArthur, and David G. Castner, *Langmuir* **18**, 4090 (2002).
- ⁴²Nan Xia and David G. Castner, *J. Biomed. Mater. Res.* **67**, 179 (2003).
- ⁴³Roger Michel, Stephanie Pasche, Marcus Textor, and David G. Castner, *Langmuir* **21**, 12327 (2005).
- ⁴⁴James R. Hull, Glen S. Tamura, and David G. Castner, *Biophys. J.* (submitted).
- ⁴⁵V. Franz, S. Loi, H. Muller, E. Bamberg, and H.-J. Butt, *Colloids Surf., B* **23**, 191 (2002).
- ⁴⁶Andres F. Oberhauser, Carmelu Badilla-Fernandez, Mariano Carrion-Vazquez, and Julio M. Fernandez, *J. Mol. Biol.* **319**, 433 (2002).
- ⁴⁷Matteo Conti, Gabriele Donati, Giuseppe Cianciolo, Sergio Stefoni, and Bruno Samori, *J. Biomed. Mater. Res.* **61**, 370 (2002).
- ⁴⁸Pamela Y. Meadows, Jason E. Bemis, and Gilbert C. Walker, *Langmuir* **19**, 9566 (2003).
- ⁴⁹P. Harder, M. Grunze, R. Dahint, G. M. Whitesides, and P. E. Laibinis, *J. Phys. Chem. B* **102**, 426 (1998).
- ⁵⁰Kevin L. Prime and George M. Whitesides, *J. Am. Chem. Soc.* **115**, 10714 (1993).
- ⁵¹Erkki Ruoslahti, *Annu. Rev. Biochem.* **57**, 375 (1988).
- ⁵²P. T. Toy and M. E. Reid, *J. Clin. Pathol.* **37**, 951 (1984).